On the Response of Radar-Derived Properties to Hygroscopic Flare Seeding

YAN YIN,* ZEV LEVIN, TAMIR G. REISIN,+ AND SHALVA TZIVION

Department of Geophysics and Planetary Sciences, Raymond and Beverly Sackler Faculty of Exact Sciences, Tel Aviv University, Ramat Aviv, Israel

30 May 2000 and 27 March 2001

ABSTRACT

Numerical calculations using a cloud model with detailed microphysics are conducted to investigate the possible effects of hygroscopic flare seeding on the changes in the spectra of hydrometeors and the resulting radar-derived properties, such as storm rain mass, rain flux, and rainfall amount. The results indicate that, in continental clouds, seeding can significantly change the distribution functions of the precipitation particles, the radar reflectivity–rainfall (Z–R) relationship, and the radar-derived properties. Therefore, different Z–R relationships derived respectively from unseeded and seeded clouds should be used to estimate properly the effects of seeding with hygroscopic flares. The results also show that the effects of hygroscopic seeding on maritime clouds are small and there is little difference in the Z–R relationship and the precipitation properties between the seeded and the unseeded cases.

1. Introduction

The evaluation of seeding effects is a difficult task, especially when operations are designed to increase precipitation from individual clouds, as is the case in experiments using hygroscopic flares. The usual way of evaluating the effect of seeding on individual clouds is to compare the rainfall from them with that falling from otherwise comparable unseeded clouds, with the seeding decision being made on a random basis. This comparison is often unsatisfactory even for clouds in the same region because of the natural variations of the clouds' parameters.

Recently, radar-derived properties have been used as the main parameters to evaluate seeding effects by hygroscopic flares. In some of these experiments, significant increases in radar-derived rain flux, total storm rain mass, storm volume and area, and so on, were reported, indicating possible rain enhancement induced by cloud seeding (e.g., Mather et al. 1996, 1997; Bigg 1997; Bruintjes et al. 1998).

In estimating rainfall R based on radar reflectivity Z to evaluate the results of a cloud-seeding experiment, it is tacitly assumed that the underlying Z–R relationship that was selected to represent best the rainfall from natural clouds would not be altered by seeding. However, one of the main objectives in hygroscopic seeding is the early production of relatively large drops that rapidly grow to precipitation-size particles, modifying the hydrometeors' size spectra and, therefore, changing the Z–R relationship. As a consequence, using an inappropriate Z–R relationship could lead to large errors in the estimation of rainfall on the ground.

This study is aimed at shedding some light on this issue. A two-dimensional numerical cloud model with detailed microphysics is used to investigate the influence of hygroscopic flare seeding on the evolution of the distribution functions of cloud and precipitation particles, the Z–R relationship, and the radar-derived properties and rainfall on the ground.

2. The model and initial conditions

The framework of the model is a two-dimensional, slab-symmetric, nonhydrostatic convective cloud model in which both warm- and ice-phase cloud microphysical processes are included and are treated explicitly using the moment method [More details of the model and related literature on the moment method can be found in Yin et al. (2000a,b)].

In this study, the grid size of the model is set to 300

* Current affiliation: School of the Environment, University of Leeds, Leeds, United Kingdom.

+ Current affiliation: Soreq Nuclear Research Center, Yavne, Israel.

Corresponding author address: Prof. Zev Levin, Dept. of Geophysics and Planetary Sciences, Tel Aviv University, Ramat Aviv 69978, Israel.
E-mail: zev@hail.tau.ac.il

TABLE 1. The values of parameters α and β used in the calculation of radar reflectivity–derived rain mass. The definitions for cases C0, C1, M0, and M1 are given in the text.

Case	α (10^{-3} g m^{-3})	β
C0	2.576	0.72
C1	1.753	0.63
M0	2.737	0.68
M1	2.385	0.67

m in both the horizontal and vertical directions. The width and height of the domain are 30 and 12 km, respectively. The time step for all the processes is 5 s except for diffusive growth/evaporation, for which a shorter time step of up to 2.5 s is used.

The radar-derived total storm rain mass, rain flux, and rainfall amount on the ground are calculated based on radar reflectivity–derived rain mass and rainfall rate at each grid point. The radar-derived rain mass M (g m^{-3}) at a certain point (x, z) and time t is calculated using a formula similar to that obtained by Morgan and Meuller (1972):

$$M(x, z, t) = \alpha Z_e(x, z, t)^{\beta}, \quad (1)$$

where Z_e is the effective radar reflectivity factor (mm^6 m^{-3}). The values of parameters α and β, obtained by fitting the model-calculated rain mass and effective reflectivity factor to this formula, are given in Table 1.

The rain flux at a certain level and time t is calculated as

$$\mathrm{RF}(z, t) = \int_A R(x, y, z, t)\, dA, \quad (2)$$

where A is the rain area and $R(x, y, z, t)$ is the radar reflectivity–derived rainfall rate, which is derived by fitting the model output reflectivity and rainfall-rate data to a formula having a similar form (see next section) as that of Marshall and Palmer (1948). (In calculating the integrated quantities such as total storm rain mass, rain flux, and rainfall amount, the cloud properties are assumed to be uniformly distributed in the y direction and the width of precipitation to be normalized is assumed to be 1 km.)

The above-mentioned radar-derived properties evaluated at one grid level above the surface are compared with those calculated directly from the model based on the size distributions and the terminal velocities of the precipitation particles and on the dynamic field.

The initial profiles of temperature, humidity, and background cloud condensation nuclei (CCN) are similar to those used by Yin et al. (2000a). A theoretical thermodynamic profile that produces clouds with cloud base at 8°C and tops at −25°C is adopted. (Note that the sounding used to initiate the model is not representative of the South African environment; therefore, the clouds that are simulated, as described in section 3a, are not typical of those selected for the South African experiment.)

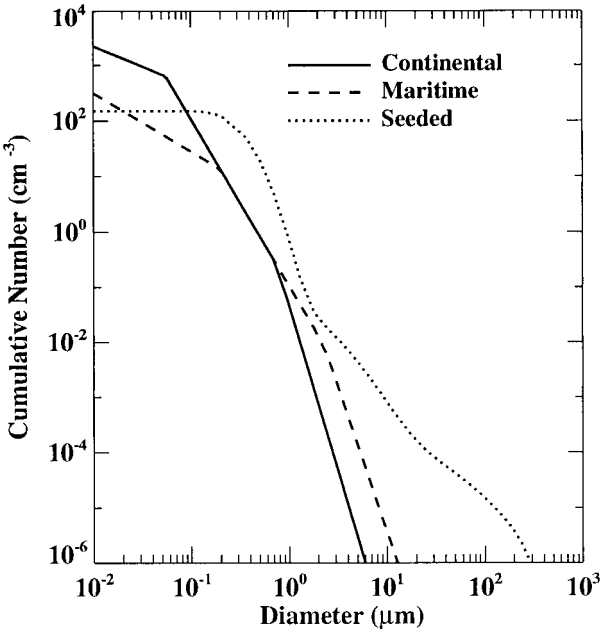

FIG. 1. Distributions of initial CCN and seeding particles from the flares.

To initiate the cloud, a temperature perturbation of 2°C is applied for one time step at $t = 0$, at a height of 600 m in the middle of the domain. Two initial background CCN spectra, with concentrations (at 1% supersaturation) of 1000 and 100 cm^{-3}, are considered to represent cloud formation in continental (C) and maritime (M) air mass, respectively.

Based on field measurements in South Africa (e.g., Mather et al. 1997; Cooper et al. 1997), the chemical composition of seeding particles is assumed to be potassium chloride, and the measured size distribution is fitted using three lognormal distribution functions. The spectra of initial background CCN and seeding particles are shown in Fig. 1.

3. Results

Four numerical experiments were conducted and are reported in this paper. Cases C0 and M0 represent the unseeded clouds developed in continental and maritime air masses, respectively. Experiments C1 and M1, respectively, represent the same cases, but seeded.

a. A brief description of the unseeded clouds

The general features of the macrostructure of these two kinds of clouds at the developing stage are similar; cloud droplets begin to appear after 23 min of simulation and rapidly reach their maximum concentrations about 14 min later. The maximum updraft remains small (less than 2 m s^{-1}) until 28 min; thereafter, the clouds experience a rapid developing phase and reach their peak value, 13 m s^{-1}, after 44 min of simulation. The max-

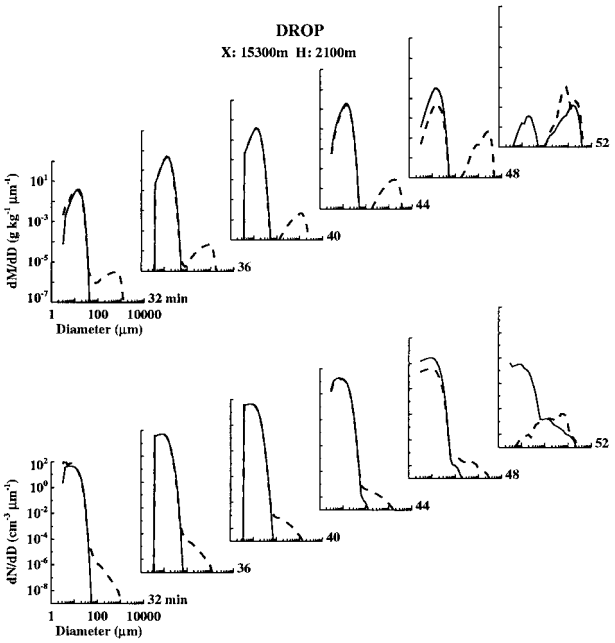

FIG. 2. (top) Mass and (bottom) number distributions as a function of time at the lower part of the cloud in the unseeded (solid line) and seeded (dashed line) continental cloud cases C0 and C1 (the location is indicated on the top).

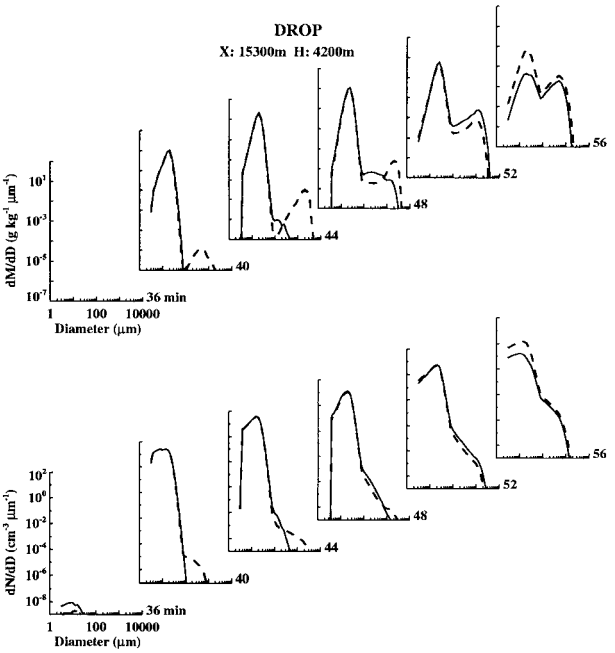

FIG. 3. Same as Fig. 2, but at the middle altitude of the cloud.

imum liquid water content of these clouds is 4.3 g kg^{-1}, the cloud base is at 1.5–1.8 km, and the cloud top is at 6.6 km above the ground. The width of the main updraft at the cloud base is about 1.2 km.

Significant differences are observed in the development of precipitation particles, radar reflectivity, rainfall rate, and rain amount in these two clouds. The specific mass and concentration of raindrops and graupel particles, radar reflectivity, and rainfall rate develop faster and achieve higher values in the maritime cloud (case M0) than in the continental one (case C0). In case M0 rain begins 47 min from model initiation and reaches a maximum rainfall rate of 158 mm h^{-1}. The maximum accumulated rain on the ground is 20 mm, and the integrated rain amount (the width of precipitation area in the *y* direction is normalized to 1 km) is 25 kilotons (kt). In case C0, rain is initiated 8 min later than in case M0 (22 min from cloud initiation) and lasts only 20 min. The rainfall rate is considerably lower, and the rain amount is reduced, with a maximum accumulated rain of only 1 mm and an integrated rain amount of 3 kt.

In the seeding cases, denoted as C1 and M1, the full spectrum of seeding particles from the flares is introduced at cloud base between 29 and 33 min of simulation (this is the optimal seeding time for these clouds).

b. Analysis of distribution functions

1) CONTINENTAL CASES C0 AND C1

Figures 2 and 3 show the evolution of mass and number concentration distributions of drops in cases C1 and C0, at the lower (2100 m) and middle regions (4200 m) of the cloud. In comparing Figs. 2 and 3 it becomes clear that in C0 drizzle or rain drops (diameter larger than 100 μm) first appear in the mid- or upper part of the cloud after 44 min of simulation and then at the lower altitude (2.1 km) between 48 and 52 min. On the other hand, in C1 similar-sized particles appear at the bottom of the cloud shortly after the seeding period (29–33 min), and only after 38–40 min do such particles appear at the higher altitudes. These results reveal that, in the unseeded clouds, the majority of the small droplets formed after nucleation are carried up during the cloud-developing stage and the growth of these droplets to raindrops mainly occurs in the middle to upper parts of the cloud. In contrast, in the seeded case, because of the competitive edge of some of the large seeding nuclei over the natural ones, larger drops form earlier and nearer to the cloud base, followed by their rapid growth via the collision–coalescence process. These larger drops fall out early, and by 44–48 min their concentration decreases. At around 40 min, many of the smaller drops from the seeded material (many of them are still larger than the natural ones) are lifted from the lower reaches of the cloud to the 4200-m level. They grow by collection and maintain the reservoir for the raindrops at the lower altitude. At about 50 min, the largest drops have already fallen, and the shape of the size distribution begins to resemble that of the natural case.

The evolution of the distributions of the graupel particles in case C1 versus case C0 is shown in Fig. 4. Consistent with the growth of raindrops, graupel particles also appear more than 4 min earlier in case C1 than in C0. In C1, graupel particles first appear before

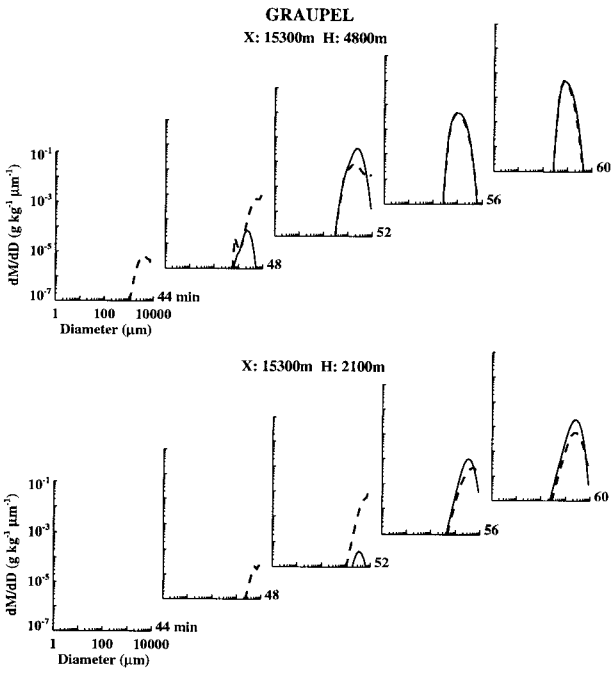

FIG. 4. Size distributions of graupel particles at different times and two locations in the unseeded (solid line) and seeded (dashed line) continental cloud cases C0 and C1.

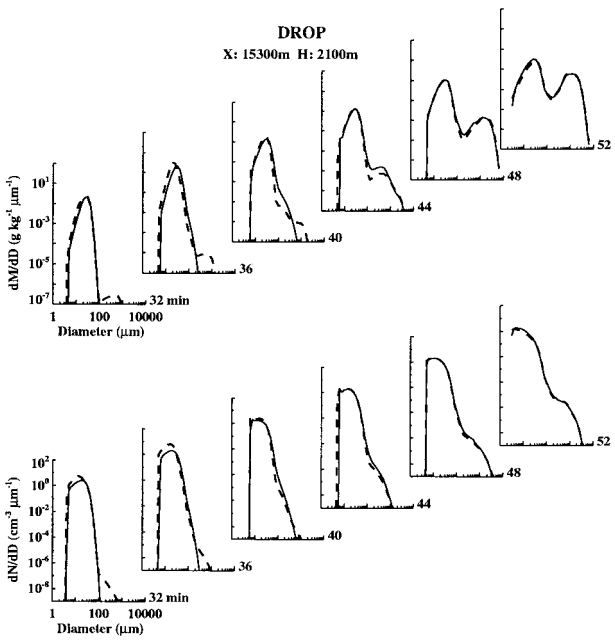

FIG. 5. Same as Fig. 2, but for maritime cloud cases M0 and M1.

44 min at the higher levels. After their descent, they appear about 4 min later at the 2100-m level. The graupel particles resulting from seeding dominate the spectrum at higher levels until about 50 min; the graupel spectra in both seeded and unseeded clouds are similar after that.

2) MARITIME CASES M0 AND M1

The evolution of raindrop size distributions in cases M0 and M1 is shown in Fig. 5. The development of the drop size distribution in the maritime cloud is considerably different from that in the continental case. Seeding produces a few larger drops near cloud base, as compared with the unseeded case (between 32 and 38 min). After about 40 min, however, the distributions in the two cases become similar. It is pointed out that because some of the seeding particles are smaller than the natural ones, higher concentrations of smaller drops are produced, leading to slightly slower growth rates and the production of slightly lower concentrations of large drops at 44 and 48 min.

Figure 6 shows the mass and number distributions of graupel particles as a function of time. As compared with the continental cases (Fig. 4), seeding a maritime cloud has a smaller effect on the development of ice-phase precipitation particles.

c. The effect of seeding on the radar reflectivity

The effect of seeding on the growth of the particles in the clouds can be seen through their influence on the radar reflectivity. Figure 7 shows the radar reflectivity as a function of height and time. In the continental cloud, seeding produces an early echo with a maximum at about 45 min at a height of about 4.5 km. The 30-dBZ contour starts near 4-km height (about $-11°C$) at about 40 min and remains so until about 70 min—much longer than the lifetime of the 30-dBZ contour in the unseeded case (from 45 to 65 min). In other words, seeding ini-

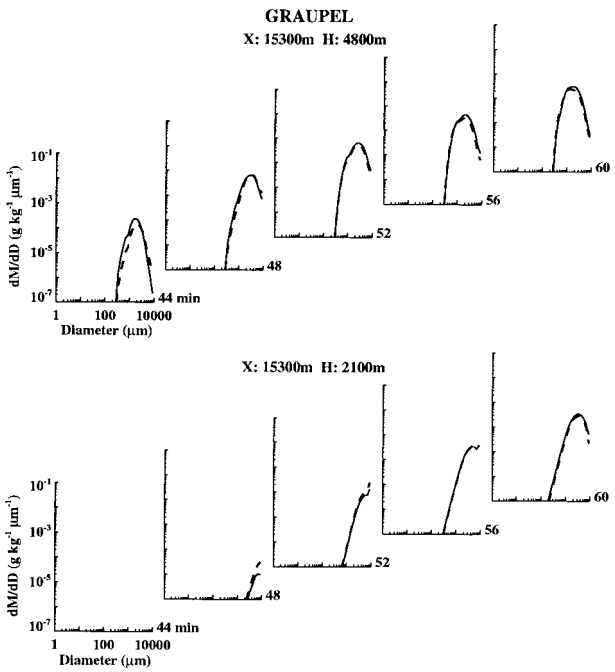

FIG. 6. Same as Fig. 4, but for maritime cloud cases M0 and M1.

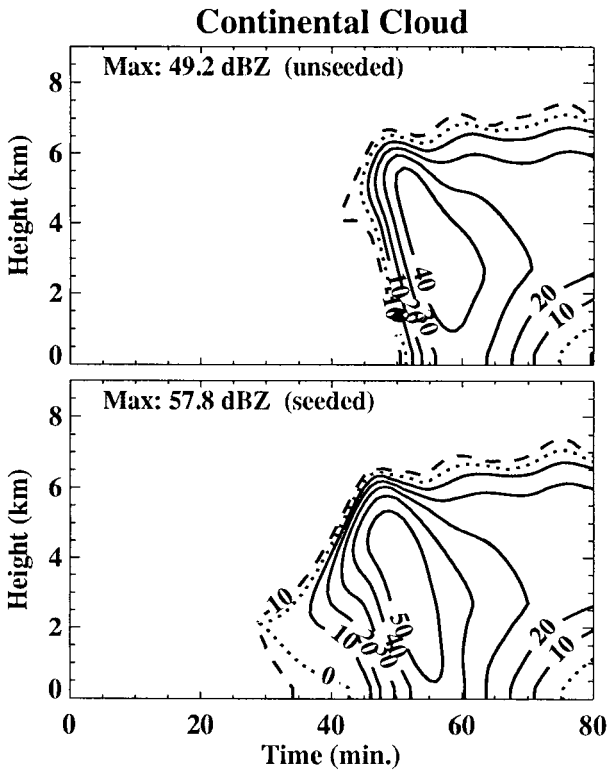

FIG. 7. Radar reflectivity at the cloud center as a function of height and time in the continental cases C0 and C1.

tiates the rain earlier, produces more rain on the ground, and lasts longer. This result is in agreement with the observations of Mather et al. (1996) and of Bruintjes et al. (1998), who used an objective radar tracking at a height at which temperature was about −11°C. In contrast to the increases in the continental clouds, the effect of seeding on the maritime clouds is very small. The maximum reflectivity increases from about 62 to 63 dBZ (not shown here).

d. The effect of seeding on Z–R relationship

The Marshall–Palmer formula is the one most often used for estimating rainfall rates from radar measurements (e.g., Mather et al. 1996). However, it is not realistic to expect that the same formula can be used for both seeded and unseeded cases because the main effect of the hygroscopic seeding is to enhance the production of large particles, implying that the size distribution of the particles in the clouds will become wider. To test the effects of the size spectra on the *Z–R* relationship, we calculated the time variations of the parameters in the formula $Z_e = A(t)R^{B(t)}$, where Z_e is the effective reflectivity factor ($mm^6\ m^{-3}$), and A and B are parameters. Figure 8 shows these values for both continental and maritime clouds. As can be seen, in the continental case, A grows initially from 50 to about 55 min and steadily decreases after that time. Although the value of A in the unseeded case is always lower than in the seeded one, the deviations are small after about 55 min. The parameter B (the exponent) deviates much more. It grows from 50 to 65 min and then decreases. In the unseeded case, the value of B increases sharply around 55 min and then remains fairly constant. The figure illustrates that the values of B in the seeded and unseeded continental clouds become similar after about 60 min during the final decaying stages of the rain. The merging of the two cases is also demonstrated in Fig. 2 in which the size spectra of the drops at 2100 m in the two clouds become similar late in the lifetime of the clouds. In the maritime clouds on the other hand, the values of A and B in the seeded and unseeded cases are much closer to each other, in agreement with the similarity of the distributions shown in Fig. 5. The dashed lines in the figures represent the constant values of the parameters A (200 $mm^6\ m^{-3}$) and B (1.6) suggested by Marshall and Palmer (1948).

Figure 9 shows a comparison of the *Z–R* relationship between seeded and unseeded cases. The lines are derived by fitting the radar reflectivity at 300-m level and rainfall-rate data on the ground (Fig. 8) using a formula of the form $Z_e = AR^B$. These figures indicate that seeding continental clouds with hygroscopic particles significantly modifies the temporal variations of the size spectra of the hydrometeors and consequently modifies the connection between Z and R (also *M–Z* relationship; see Table 1). This effect is primarily true in the lower regions that are the most important for estimating rainfall on the ground.

e. The effect of seeding on radar reflectivity–derived properties

1) CONTINENTAL CASES C0 AND C1

Figure 10 shows the total storm rain mass (kt), rain flux ($m^3\ s^{-1}$), and integrated rainfall amount ($10^3\ m^3$) on the ground, calculated based on the rain mass and rainfall rate derived from radar reflectivity (RD, thin lines) using the *Z–R* relationships shown in Fig. 9, as well as those calculated explicitly in the model (MC, thick lines), for cases C0 and C1. The results obtained in the seeded case by using the same *Z–R* relationship derived from the unseeded cloud (as is most often done in the field) are also shown in the figure as a dash–dot line (RD2). The figure shows that there are differences between the reflectivity-derived (RD) precipitation properties (total storm rain mass, rain flux, and rainfall amount) and the model-calculated ones (MC) because a constant *Z–R* relationship (shown in Fig. 9) is used. This difference could, in principle, be reduced through the use of time-dependent *Z–R* relationships that fit the data in Fig. 8. Despite the discrepancies, it is noted that the ratio of the seeded to unseeded precipitation properties based on RD estimates compares well with those based on MC. As an example, Table 2 shows the total

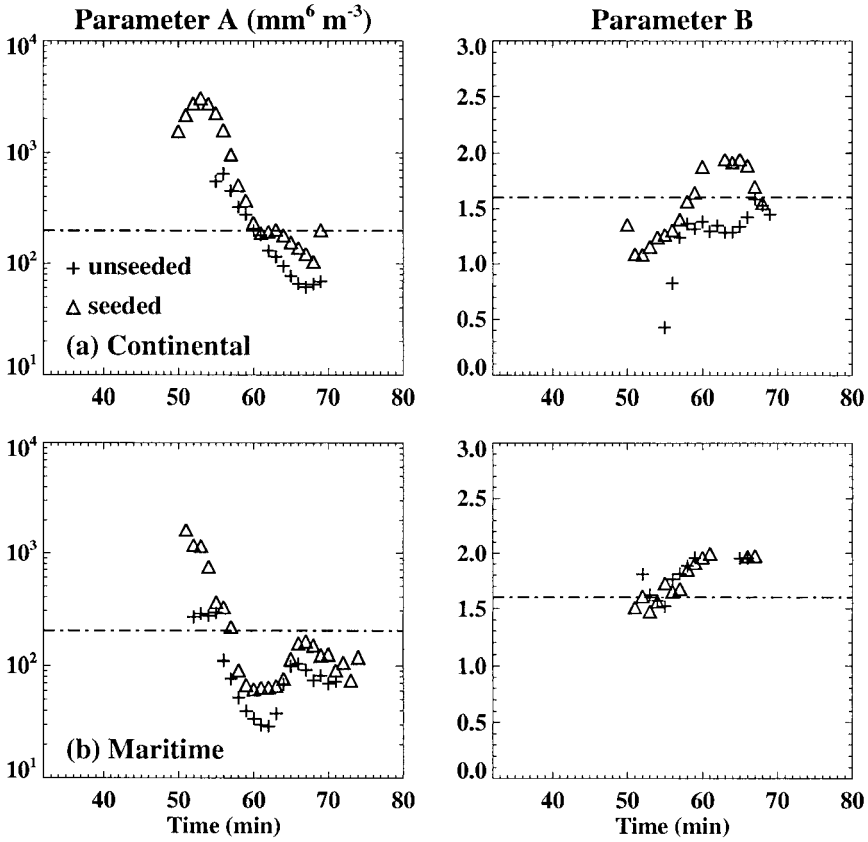

FIG. 8. Variation of the parameters A and B in formula $Z(e) = A(t)R^{B(t)}$ as a function of time in the four simulated cases.

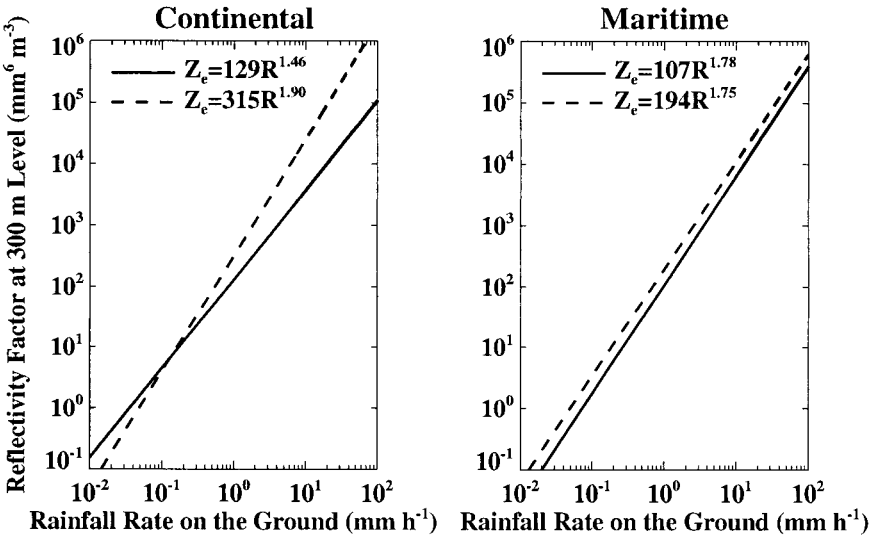

FIG. 9. The Z–R relationship calculated from the unseeded and seeded continental and maritime clouds. The equations used to plot the lines are also given.

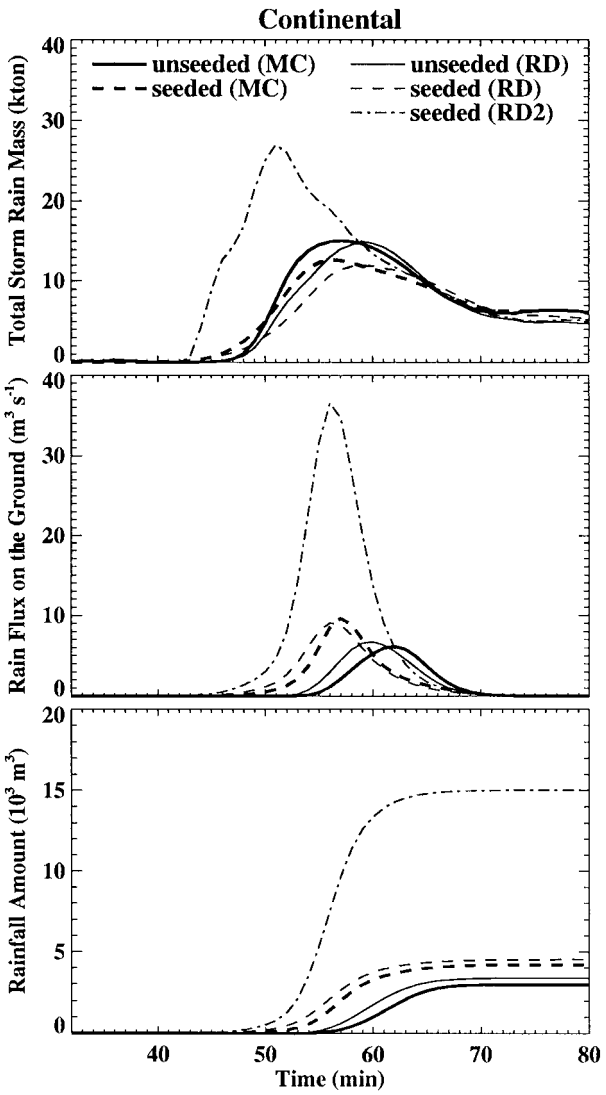

FIG. 10. The total storm rain mass (kt), rain flux ($m^3\ s^{-1}$), and integrated rainfall amount ($10^3\ m^3$) calculated explicitly in the model (MC, thick lines) and those derived from radar reflectivity (RD, thin lines) in the unseeded (solid lines) and seeded (dashed lines) continental cloud cases C0 and C1. The dash–dot lines represent the results obtained in the seeded case using the *Z–R* relationship from the unseeded case (RD2). When calculating the total storm rain mass and integrated rainfall amount, the width of the precipitation region in the *y* direction was normalized to be 1 km.

rainfall amount after 80 min of simulation and the ratios between the seeded and unseeded clouds. The ratio of rainfall amount in seeded to unseeded clouds based on estimation from RD is similar to the ratio based on MC (the slight difference results from the use of constant *Z–R* relationships in the RD estimation). This finding indicates that the use of constant *but different Z–R* relationships derived from unseeded and seeded clouds, respectively, can be used for determining whether a seeding experiment with hygroscopic flares is successful. On the other hand, the use of the *same Z–R* relationship derived from unseeded clouds to estimate the precipitation properties from the seeded clouds (compare the dash–dot lines with the thin dashed ones) could lead to significant errors. For example, after 80 min, the ratio of the total rainfall amount between the seeded and unseeded cases is 4.44 when the same *Z–R* relationship from the unseeded cloud is used (see Table 2). This value is much larger than that (1.34) obtained using different *Z–R* relationships derived from seeded and unseeded clouds, respectively, or that (1.41) based on MC. Namely, using the *Z–R* relationship from the *same but unseeded* cloud would lead to an overestimation of the seeding effect by more than 300%.

TABLE 2. Total rainfall amount and ratios between the seeded and unseeded continental cloud after 80 min of simulation. Here, MC represents the values directly calculated in the model based on particle size spectra; RD represents reflectivity-derived values by using constant but different *Z–R* relationships from unseeded and seeded cases; RD2 represents reflectivity-derived values using the same constant *Z–R* relationship from the unseeded cloud.

Case	Unseeded ($10^3\ m^3$)	Seeded ($10^3\ m^3$)	Seeded/unseeded
MC	2.99	4.21	1.41
RD	3.39	4.53	1.34
RD2	3.39	15.03	1.44

Both RD and MC values in Fig. 10 indicate that the storm rain mass increases earlier in case C1 than in C0, consistent with the early evolution of large drops in the seeded case (e.g., Fig. 2). The peak values of the total storm rain mass are smaller in the seeded case C1 than in the unseeded one, however, as a result of the fact that the larger drops formed in the seeded cases fall out early, as expressed by the larger rainfall rate or rain flux. Bigg (1997) suggested that the stronger rain flux would produce stronger downdrafts that could enhance the subsequent development of nearby updrafts and of other clouds in the region, leading to more rain on the ground. These secondary processes are not simulated in this work, although the model does show the development of stronger downdrafts during the period of heaviest rainfall (results not shown).

2) MARITIME CASES M0 AND M1

The evolution of the total storm rain mass, rain flux, and integrated rainfall amount in the maritime cases M0 and M1 is shown in Fig. 11. As compared with the continental cases C0 and C1, the changes induced by seeding are less pronounced in this maritime cloud. The main difference between M1 and M0 is that the increased number of droplets introduced by seeding reduces the efficiency of precipitation, leading to a slight decrease in the total storm rain mass, rain flux, and total rainfall on the ground. Again, the radar reflectivity–derived values are in relatively good agreement with those calculated explicitly in the model. Figure 11 also indicates that the precipitation properties in the seeded

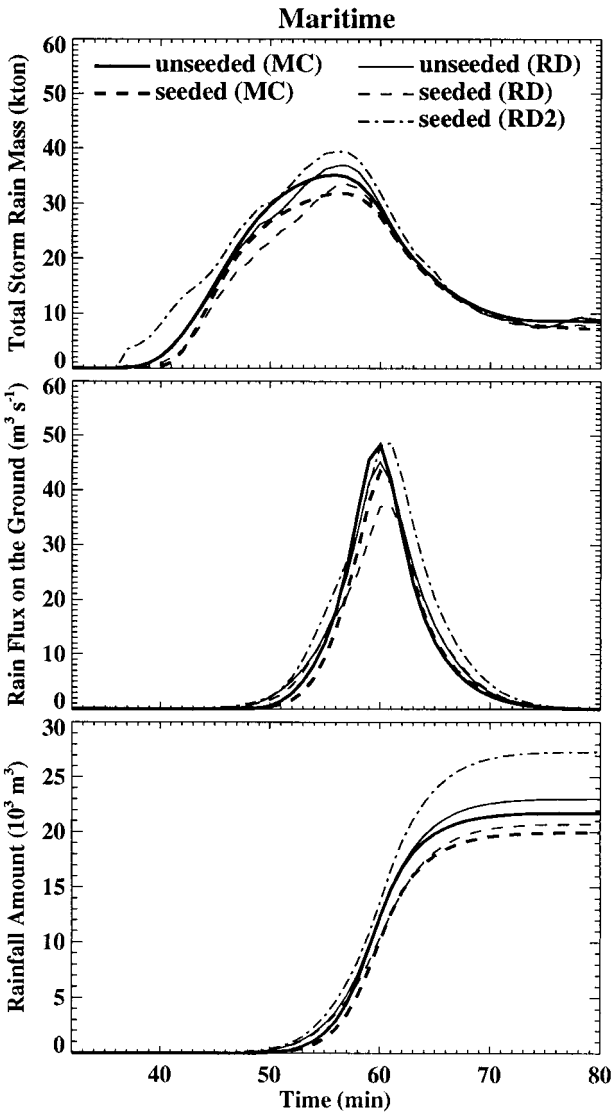

FIG. 11. Same as Fig. 10, but for maritime cloud cases M0 and M1.

case calculated using the *Z–R* and *Z–M* relationships derived from the unseeded case (the dash–dot lines) are much closer to the results obtained using the *Z–R* and *Z–M* relationships from the seeded case (the dashed lines), as compared with the continental case.

4. Conclusions

The results obtained in this numerical experiment indicate that, in continental clouds, hygroscopic seeding with flares can change significantly the distribution functions of the precipitation particles and relationship between radar reflectivity *Z* and rain rate *R*. Therefore, *different Z–R* relationships derived from unseeded and seeded clouds should be used to estimate the effects of seeding with hygroscopic flares. It is also shown that a reasonable estimate of seeding effect with hygroscopic flares can be achieved by using a constant *but different Z–R* relationship derived from unseeded and seeded clouds, respectively, and that the estimation could be very much improved through the use of time-dependent *Z–R* and *Z–M* relationships. On the other hand, using a constant *Z–R* relationship obtained from the unseeded clouds to estimate the rain enhancement in seeded clouds could lead to large errors. In the case simulated here, an overestimation of about 300% in the seeding effects is obtained.

The results also indicate that the effects of hygroscopic seeding on maritime clouds are small and there is little difference in the *Z–R* relationship and the precipitation properties between the seeded and the unseeded cases.

Acknowledgments. We thank the Israel Water Commissioner for partially funding this research. Thanks are also due to Mr. Louis and the late Mrs. Florence Ross for their contribution to the laboratory, which made part of this work possible. Part of the calculations were conducted on the Cray J932 computer of IUCC of Israel.

REFERENCES

Bigg, E. K., 1997: An independent evaluation of a South African hygroscopic cloud seeding experiment, 1991–1995. *Atmos. Res.*, **43,** 111–127.

Bruintjes, R. T., D. W. Breed, M. J. Dixon, B. G. Brown, V. Salazar, and H. R. Rodriguez, 1998: Program for the Augmentation of Rainfall in Coahuila (PARC): Overview and preliminary results. Preprints, *14th Conf. on Planned and Inadvertent Weather Modification*, Everett, WA, Amer. Meteor. Soc., 600–603.

Cooper, W. A., R. T. Bruintjes, and G. K. Mather, 1997: Calculations pertaining to hygroscopic seeding with flares. *J. Appl. Meteor.*, **36,** 1449–1469.

Marshall, J. S., and W. M. K. Palmer, 1948: The distribution of rain drops with size. *J. Meteor.*, **5,** 165–166.

Mather, G. K., M. J. Dixon, and J. M. de Jager, 1996: Assessing the potential for rain augmentation—the Nelspruit randomized convective cloud seeding experiment. *J. Appl. Meteor.*, **35,** 1465–1482.

——, D. E. Terblanche, F. E. Steffens, and L. Fletcher, 1997: Results of the South African cloud-seeding experiments using hygroscopic flares. *J. Appl. Meteor.*, **36,** 1433–1447.

Morgan, G., and E. A. Meuller, 1972: The total liquid water mass of large convective storms. Preprints, *15th Radar Meteorology Conf.*, Champaign, IL, Amer. Meteor. Soc., 39–40.

Yin, Y., Z. Levin, T. G. Reisin, and S. Tzivion, 2000a: Seeding convective clouds with hygroscopic flares: Numerical simulations using a cloud model with detailed microphysics. *J. Appl. Meteor.*, **39,** 1460–1472.

——, ——, ——, and ——, 2000b: The effects of giant cloud condensation nuclei on the development of precipitation in convective clouds—a numerical study. *Atmos. Res.*, **53,** 91–116.